Journal of Colloid and Interface Science 576 (2020) 376–384

Contents lists available at ScienceDirect

Journal of Colloid and Interface Science

journal homepage: www.elsevier.com/locate/jcis

Control over electroless plating of silver on silica nanoparticles with sodium citrate

Jeffrey E. Chen [a,b], Qifeng Wang [b], Kenneth R. Shull [b], Jeffrey J. Richards [a,*]

[a] Department of Chemical and Biological Engineering, Northwestern University, Evanston, IL 60208, USA
[b] Department of Materials Science and Engineering, Northwestern University, Evanston, IL 60208, USA

GRAPHICAL ABSTRACT

Three step synthesis route to forming silver coated silica nanoparticles with citrate as a key ingredient to achieving morphological control.

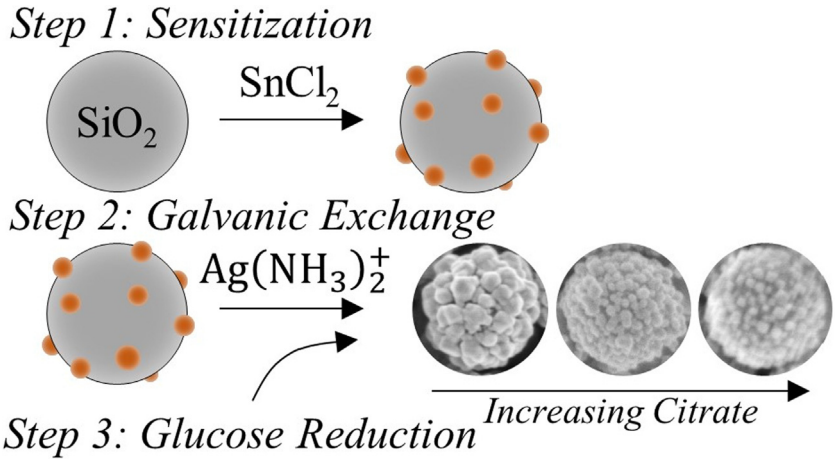

ARTICLE INFO

Article history:
Received 17 January 2020
Revised 5 May 2020
Accepted 7 May 2020
Available online 11 May 2020

Keywords:
Electroless plating
Silver
Silica
Nanoparticle
Sodium citrate
Capping agent
Complexing agent

ABSTRACT

We describe the use of citrate to control the electroless plating of silver metal on silica nanoparticles. We find that the incorporation of relatively small amounts of citrate during the reduction of the Tollens' reagent in the presence of sensitized silica nanoparticles induces a continuous transition from conformal to raspberry particle coatings. This transition is dependent on both the citrate concentration and the silver precursor concentration. We characterize this transition using electron microscopy and spectroscopy and use these results to confirm citrate's ability to cap and restrict silver growth. We compliment these structural measurements with in-situ quartz crystal microbalance experiments to quantify citrate's role as a complexing agent to slow silver reduction kinetics. These results confirm citrate's dual role in controlling the morphology of silver deposits produced in this work.

* Corresponding author at: McCormick School of Engineering, Technological Institute, 2145 Sheridan Road, Evanston, IL 60208, USA.

https://doi.org/10.1016/j.jcis.2020.05.024
0021-9797/

1. Introduction

The deposition of silver metal is an important processing step used in the creation of microelectronic interconnects [1,2], sensors [3], wearable electronics [4], and photonic metamaterials [5,6]. While vacuum processes are common deposition techniques for these applications, electroless plating is an attractive alternative [7]. Electroless plating of silver metal involves the chemical reduction of a silver precursor to form metallic silver deposits on pretreated surfaces. This process has been used for decades to produce mirrors [8]. Electroless plating has gained renewed attention for nanoscale manufacturing due to its potential to deposit silver conformally onto nanosized features, complex geometries [6], and nano- and micro-particles [9,10]. In the chemical deposition of silver on such surfaces [11-14], it is highly desirable to control the coating properties. If the morphology of the silver deposits can be controlled, then the conductivity [4,15,16], plasmonic properties [17–19], antibacterial potency [20], and catalytic activity [21] can be designed for various applications. However, controlling the morphology of silver deposits during electroless plating remains challenging [22].

A common strategy for controlling morphology during electroless plating is the incorporation of surfactants or capping agents in the reacting mixture [4,11–14,23–26]. The presence of these surface active agents can modify the way the silver crystallites grow, altering their grain size and crystal habit. However, in some cases, the presence of these chemicals after synthesis can have a deleterious effect on the metal's optical and electrical properties [27]. Therefore, it is desirable that the surfactant be removed post-synthesis. Citrate has been used for this purpose in the synthesis of silver nanoparticles via chemical reduction and in electroless plating of silver on nanoparticles surfaces [21,28,29]. Citrate is an effective capping agent for silver metal and also binds reversibly to the silver metal surface. An added benefit of citrate in nanoparticle synthesis is that it imparts a negative surface charge that improves the colloidal stability of the nanoparticle product.

Citrate has been extensively used to modify electro- and electroless- deposition of Cu [30,31], ZnS [32], Ni [33], CuInSe2 [34-36], and InSb [37] thin films. In general, it is observed that citrate slows the rate of the plating reaction resulting in more sparse deposits. However, it is less frequently employed in silver electroless plating. Recent work by Chen et al has shown that the addition of citrate during electroless plating resulted in denser and more conformal silver films on the surface of polystyrene latex particles. They concluded that the film quality of the silver deposits depended in part on the timing of citrate's addition and the duration of the synthesis [23]. In contrast, Kobayashi used a very similar synthesis scheme without citrate and observed sparse silver deposits on spherical silica particles that grew larger and more polydisperse with increasing reduction of the silver precursor [38]. These results suggest that the addition of citrate can play a key role in determining the quality of the silver deposits formed during the reaction. However, a mechanistic understanding of how citrate modifies the growth behaviour of silver deposits has not yet been described.

In this work, we study the use of citrate as a growth modifier to control the electroless deposition of silver metal on the surface of silica nanoparticles. Our electroless plating strategy follows the approach of Chen et al. [23] with the exception that we use a trifluoroacetic acid (TFA) and stannous chloride mixture for sensitizing the silica particles following the approach of Kobayashi et al. [38]. Our approach concsists of three steps. First, the silica nanoparticles were pretreated with stannous chloride. Second, the treated silica nanoparticles were exposed to the Tollens' reagent to induce galvanic exchange of tin for silver. Finally, the Tollens' reagent was further reduced using glucose in the presence of citrate. Chen et al had identified that citrate plays a key role in producing densely packed films of silica on polystyrene surfaces. To understand the role of citrate on the film quality after electroless deposition, we characterized each step of this reaction using X-ray photoelectron spectroscopy (XPS) and transmission electron microscopy (TEM). These microstructural studies were complemented with in-situ quartz crystal microbalance (QCM) to capture the kinetics of the reaction. We also performed scanning electron microscopy (SEM) and energy dispersive X-Ray adsorption spectroscopy (EDS) to quantify morphological changes that depended on the reaction conditions. In general, we observed that in the presence of citrate our approach yielded conformally coated silica nanoparticles whose morphology depended both on the initial Tollens' reagent concentration and concentration of citrate in the reacting mixture. As the concentration of citrate in the reacting solution was increased, we observed a morphological transition from conformal coatings to discrete nanoparticles (we refer to these particles as raspberry) on the silica surface that increased in number density and size with increasing reaction time and Tollens' reagent concentration. We use these results to show that citrate played a dual role in determining the growth morphology by both capping the growth of the silver crystallites, preventing their fusion into conformal films, and slowing the rate of reduction of the silver precursor.

2. Experimental

Materials: D-(+)-Glucose (ACS reagent), cetyltrimethylammonium chloride (25 wt% in H2O), sodium dodecyl sulphate (ACS reagent, ≥99.0%), citrate dihydrate (≥99%, FG), trifluoroacetic acid (TFA) (Reagent Plus, 99%), ethanol (200 proof, ACS reagent, ≥99.5%), potassium hydroxide (ACS Reagent, ≥85%, pellets), and tetraethyl orthosilicate (TEOS) (Reagent grade, 98%) were purchased from Sigma Aldrich. Tin (II) chloride (anhydrous, 99% min) was purchased from Alfa Aesar. Ammonia solution 28–30% was purchased from Merck. Deionized water (ACS Reagent grade, ASTM Type I) was purchased from LabChem. Methanol (certified ACS) and potassium chloride (certified ACS) were purchased from Fisher Chemical. All reagents were used as received.

Synthesis of silica nanoparticles: Silica nanoparticles were synthesized by the well-known Stöber process [39]. Briefly, 176 mL of ethanol and 24 mL of ammonia were added to a 250 mL round bottom flask. A magnetic stir bar was added and set to a constant stir rate of 300 rpm. 7.2 mL of TEOS was injected, and the reaction run to full conversion for 20 h. The product was washed three times with deionized water by centrifugation at 4000 rpm for 5 min. The silica nanoparticles were finally dispersed in deionized water at a concentration of 10 mg/mL for subsequent reaction steps.

Sensitization of silica nanoparticles: To initiate the sensitization process, 1 mL of the 10 mg/mL silica dispersion was added to 9 mL of tin sensitizing solution consisting of 29 mM $SnCl_2$ and 72 mM TFA in a 50 v/v water methanol solution [38]. After initially gently shaking the mixture and waiting 30 min for sensitization to occur, the particles were washed three times with deionized water using centrifugation at 4000 rpm for 5 min. The sensitized silica nanoparticles were then resuspended in water to a final concentration of 10 mg/mL. Sensitized particles were never dried and used immediately after preparation to avoid oxidation of the sensitized product.

Preparation of silver precursor: The Tollens' reagent was prepared from a concentrated aqueous silver nitrate solution. A dilute KOH solution was added to this concentrated stock silver nitrate solution to achieve a molar ratio of [$AgNO_3$]:[KOH] = 500:1. After incorporation of the KOH, the solution turns from transparent to

a pale yellow due to the formation of silver oxide [40]. Ammonia was then added dropwise to this solution and during this addition the colour transitioned first to brown/black and then became transparent. This transition indicates the conversion to the Tollens' reagent [40]. The Tollens' reagent was then diluted with deionized water to the desired concentration. The Tollens' reagent should always be made fresh and used within the hour of its preparation due to the potential for the formation of an explosive precipitate [41].

Synthesis of silver coated silica: 1 mL of tin treated silica (10 mg/mL) was added to 9 mL of Tollens' reagent under magnetic stirring at 300 rpm for 5 min inside a cardboard box to prevent light exposure. For reactions that utilized surfactants, a concentrated solution of surfactant was added after galvanic exchange but before adding the reducing agent. For reactions that utilized citrate, a concentrated citrate solution was directly added to the glucose solution. Then, 3 mL of glucose solution (concentration adjusted for a stoichiometric ratio of 2:1 glucose to Tollens' reagent) was added to the vial to react for the remaining reaction time, which in a typical synthesis was 25 min. The particles were washed three times with deionized water with centrifugation at 4000 rpm for 5 min.

Characterization of Silver Deposition: SEM images and EDS of silver-coated particles were obtained with a Hitachi SU8030 cold source field emission scanning electron microscope in secondary electron imaging mode. The accelerating voltage was set to 2 kV with a working distance of approximately 8 mm. TEM images were obtained with a Hitachi HT7700 transmission electron microscope using an accelerating voltage of 120 kV. Scanning transmission electron microscope images of tin hydroxide colloids and silver seeded particles were obtained with a Hitachi HD2300 scanning transmission electron microscope equipped with a field emission gun operating with an accelerating voltage of 200 kV.

XPS was performed with a Thermo Scientific ESCALAB 250Xi. Zeta potential was conducted using a Malvern Instruments Zetasizer. The tin sensitized silica particles were diluted by a factor of 10 and adjusted to 1 mM KCl. Malvern Zetasizer Nanoseries disposable folded capillary cells DTS1070 were used for the measurements. Zeta potential was calculated from the electrophoretic mobility using a Matlab solver function with the equation derived by Ohshima [42,43] as depicted in S1. Particle electrical conductivity was measured with a multimeter using particle thin films (~0.67 mg/cm^2) drop casted on interdigitated gold arrays with 200 μm channel lengths (Metrohm, DropSens DRP-IDEAU200).

Mass adsorption tests were performed using a Quartz crystal microbalance (QCM) and were carried out on a customized setup with an in-situ liquid immersion cell (Advanced Wave Sensors S. L., Paterna, Spain) in conjunction with a N2PK impedance analyzer (Thornhill, Canada). SiO2 covered (Ti/Au/Ti/SiO2) quartz crystal resonators (Inficon, East Syracuse, NY) with a fundamental resonance frequency of 5 MHz were used in this study. A lab-developed open source program written with Python was used for both the data collection and analysis [44]. The electrical conductance and susceptance of the quartz crystal near each odd harmonic were collected and the Lorentz curves were fit to each resonant peak. From these fits, the resonant frequencies and bandwidths could be extracted. Resonance of the third harmonic was used for the analysis. All the frequency shifts were referenced to the bare crystal resonance frequency in corresponding solvents, respectively. For the rigid metal films, the areal mass of deposits were assumed to obey Sauerbrey equation [45]:

$$\Delta m_a = -\frac{\Delta f Z_q}{2nf_1^2} \quad (1)$$

where Δm_a is area mass of the deposited film, Δf is the shift of resonance frequency of the tested harmonic, Z_q is the shear acoustic impedance of quartz which is 8.84 × 106 kg·m^{-2}·s^{-1} for AT-cut quartz crystals, n is the harmonic tested, and f_1 is the fundamental frequency of the quartz crystal.

3. Results

Silver Deposition on Silica Nanoparticles: In order to gain insight into the mirroring reaction on silica particles, we characterized the reaction at each step of the three-step procedure. First, silica nanoparticles of 260 nm (as measured with TEM, Fig. 1a) were prepared by the Stöber method [39] and then were treated with a tin sensitizing solution to functionalize the silica surface with Sn^{2+} ions. The adsorption of Sn^{2+} ions is known to occur spontaneously and is attributed to the electrostatic adsorption of positively charged tin hydroxide colloids formed within the sensitization solution to the negatively charged silica surface [46–48]. These colloids were visible by TEM as small (3–5 nm) particles present on the silica surface after treatment in Fig. 1b. These results are identical to what was observed by Kobayashi et al. [38] The presence of tin was also shown by XPS in Fig. 1d by the Sn 3d5 peak at 486.4 eV corresponding to the literature value [38]. Although XPS analysis confirmed the presence of cationic tin species, XPS sample preparation included particle drying that is known to oxidize Sn^{2+}. Therefore, we complemented these XPS measurements with zeta potential measurements of the as prepared particles to confirm the charge of the tin species. The increase of surface charge from the native silica toward more positive values shown in Fig. S1a confirms the deposition of a cationic species on the silica surface. The change of zeta potential is a hallmark of sensitization as observed by Chen et al. [23].

The second step of the synthesis involved the galvanic exchange of stannous ions for silver. Following Chen et al and Kobayashi et al, galvanic exchange was achieved by exposing the tin sensitized silica to the Tollens' reagent based on the following equation:

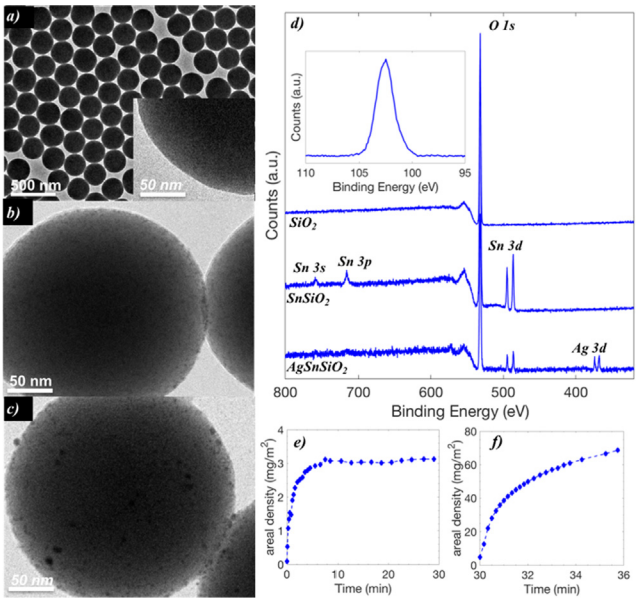

Fig. 1. TEM and STEM image of (a) as synthesized silica nanoparticles (high magnification TEM images in the inset), (b) tin sensitized silica, and (c) silver seeded silica. (d) XPS spectra of untreated silica (SiO_2), tin sensitized silica ($SnSiO_2$), and silver seeded silica ($AgSnSiO_2$) with labels underneath the corresponding spectrum. The inset shows the Si peak. In-situ QCM for the (e) Sn adsorption and (f) Ag galvanic exchange process using a SiO_2 covered (Ti/Au/Ti/SiO_2) quartz crystal resonator.

$$2Ag^{+}_{(aq)} + Sn^{2+}_{(s)} \rightarrow 2Ag_{(s)} + Sn^{4+}_{(s)} \quad (2)$$

KOH was added to the Tollens' reagent with a molar ratio of silver to potassium [$AgNO_3$]:[KOH] = 500:1 as previous studies have suggested that this increases the silvering rate and produces smoother silver films [49]. Exposure to the Tollens' reagent yielded a notable change on the silica surface as seen from TEM images in Fig. 1c. The presence of silver metal after exchange was confirmed by XPS in Fig. 1d as evidenced by the 3d5 peak at 368.9 eV corresponding to the Ag^0 literature value [38].

In-situ gravimetric measurements using QCM were performed to confirm that the sensitization time and galvanic exchange time chosen for our synthesis were appropriate. The QCM substrates consisted of planar silica sensing electrodes that were exposed to identical solution conditions as those used to treat the silica nanoparticles. The accumulation of mass associated with tin sensitization is shown in Fig. 1e and the galvanic exchange step in Fig. 1f. As seen in Fig. 1e, adsorption of the tin species saturated the substrate within 10 min of the initial exposure. Galvanic exchange was started after 30 min of sensitization time after flushing the cell and introducing freshly prepared Tollens' reagent. In Fig. 1f, galvanic exchange proceeded rapidly with complete exchange occurring after 5 min. While these measurements were performed on planar substrates, adsorption, and reaction rates onto spherical nanometer sized silica particles are much more rapid. The resulting thin-film structure is also expected to be different due to the geometric frustration expected on curved surfaces with respect to planar ones [22].

Quantification of the sensitization step can be performed by comparing zeta potential measurements in Fig. S1b to those made from the electron microscopy images and QCM measurements. Estimates for the surface coverage of tin yield 539 ± 203 positive ions per particle from zeta potential, 2800 tin species per silica nanoparticle from the QCM measurements, and approximately 1,000 tin colloids per particle from TEM measurements. The difference between the estimates for adsorbed tin is likely related to the effective charge density of the adsorbed tin species. It is thought that tin adsorbs as a colloidal particle that is formed in the sensitizing solution. These tin colloids consist of polymerized stannic oxide species that incorporate Sn^{+2} ions enriched at the colloid surface. These positively charged colloids adsorb to negatively charged surfaces and sensitize them for activation through galvanic exchange. We attribute the differences between the different measurement methods to tin colloids containing species with mixed valence including charged Sn^{+2} species versus the neutral $Sn(OH)_4$.

The adsorbed mass accumulated during the galvanic exchange step provides some insight into how galvanic exchange works to seed the mirroring reaction. Assuming comparable molar masses for the tin species and silver metal deposits, the increased mass is 10 times that expected for stoichiometric exchange of silver for tin indicated by Eq. (2). This is in line with previous experimental observations and our own TEM measurements that indicate galvanic exchange results in the deposition of silver metal nuclei. These nuclei improve adhesion and growth of the silver film on the silica surface.

In the final and third step, glucose was added to the reaction to initiate further reduction of the Tollens' reagent to silver metal. Glucose is a well-established reducing agent for the Tollens' reagent [4,16,26,50]. Glucose reduces the Tollens' reagent via the well-known aldehyde reaction [51].

$$RCHO_{(aq)} + Ag^{+}_{(aq)} \rightarrow RCOO^{-}_{(aq)} + Ag_{(s)} \quad (3)$$

The glucose concentration was chosen so that the Tollens' reagent would be limiting with a 2:1 [glucose]:[Tollens'] molar ratio. Glucose addition resulted in the rapid reaction and deposition of silver metal on the surface of the silica nanoparticles as shown in SEM images in Fig. 2a. Analysis of the micrographs yielded an average coating thickness of 110 ± 37nm. Unfortunately, excessive silver growth is apparent and resulted in bridging between multiple silica nanoparticles. We also performed a controlled synthesis where the same reaction was performed without tin sensitization to ascertain the role that sensitization and galvanic exchange (steps 1 and 2) played in the resultant morphology as shown in Fig. 2b. Silver reduction in the presence of untreated silica showed a dramatic change in the particle morphology. Whereas coatings performed with the sensitization pretreatment produced dense silver deposits, non-uniform coatings of discrete silver deposits formed without pre-treatment. This result is identical to that observed when sensitized silica was left to age for 5 days prior to the reaction as shown in Fig. S2. This aging is known to result in the oxidation of the tin species, which reduces the efficacy of galvanic exchange [16]. Based on this observation, the tin sensitized particles were kept in solution and used immediately after preparation to minimize oxidation. We speculate that the nanoparticles evident in Fig. 2b. may form by nucleating in solution first and then subsequently adsorbing to the silica surface. When sensitization is used, the solution phase reduction of the Tollens' reagent is greatly suppressed, and the silver predominantly grows on the silica surface.

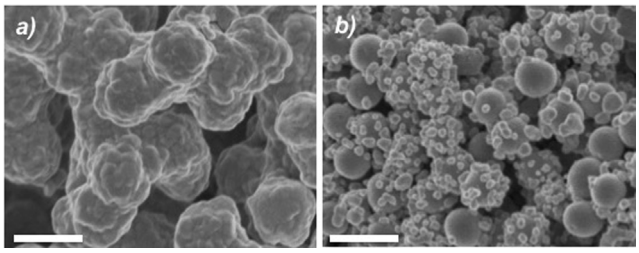

Fig. 2. SEM images of silver-coated silica after glucose reduction (a) using a tin sensitized silica core and (b) an unsensitized silica core. [Tollens'] = 50 mM for these conditions. Scale bar is 500 nm.

Controlling Silver Coating Morphology with Citrate: Chen et al showed that citrate promotes colloidal stability during electroless deposition by imparting the growing metal particles with a negative surface charge [23]. We explored several surfactants and capping agents in addition to citrate that have been reported in the literature to modify the morphology of the silver nanoparticles as outlined in a summary provided in the supplemental information and Fig. S3. Our survey showed that citrate was the most effective at stabilizing the silver-coated silica particles. Our survey also indicated that the concentration of citrate was a key variable to achieving the improved stability. In order to explore further the effect of changing citrate concentration, we varied both the Tollens' reagent concentration (25 mM, 50 mM, 100 mM, and 200 mM) and citrate concentration (0, 0.05 mM, 0.5 mM, 2.5 mM, 5 mM, 50 mM) in the silver mirroring reaction. The resulting effect on the morphology is shown in Fig. 3. Citrate was directly added to the glucose reducing solution before introduction of the Tollens' reagent. Without the addition of citrate, the coating morphology appeared overgrown and the particles were significantly bridged. In general, citrate had a dramatic influence on the morphology observed over all concentrations of Tollens' reagent tested. By increasing the citrate concentration while holding the Tollens' reagent concentration fixed, the coating morphology transitioned from dense and uniform coatings of bridged particles to conformally coated films and finally to sparsely coated raspberry particles at high citrate concentrations. The concentration of citrate necessary to induce this transition increased with increasing Tollens' reagent concentration. The region where conformal, bridged

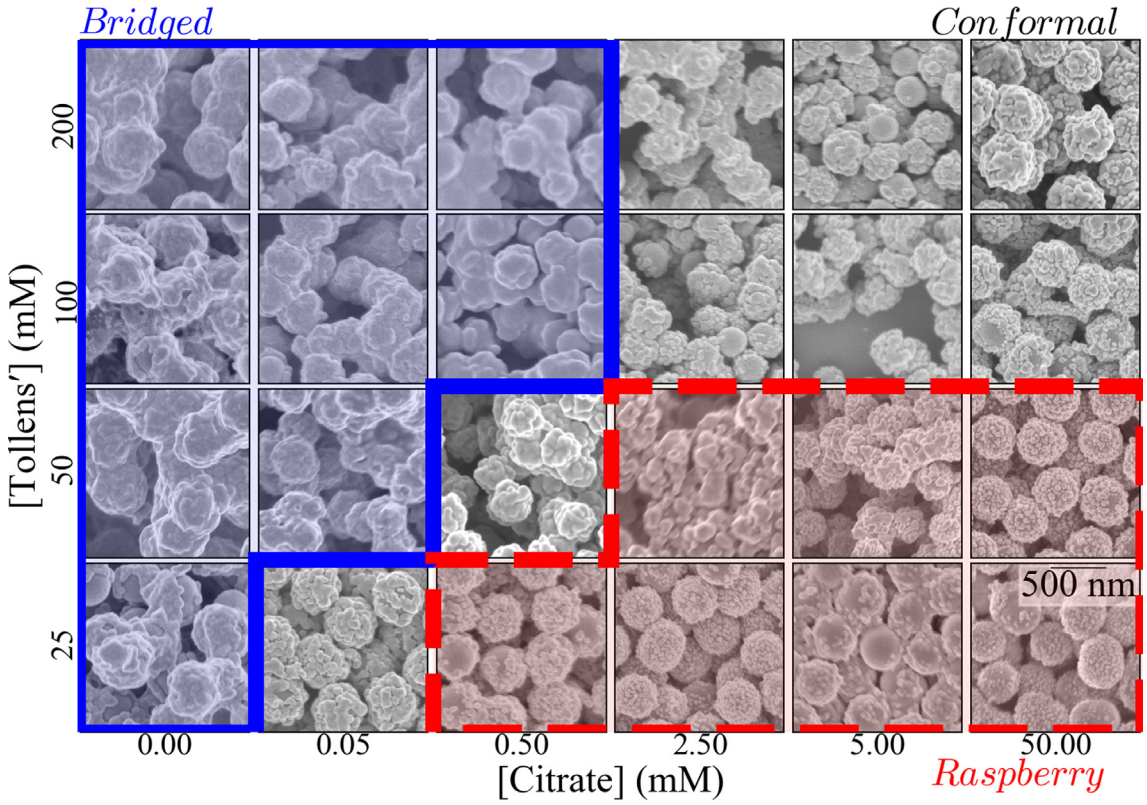

Fig. 3. SEM images of silver-coated silica nanoparticles synthesized with varying concentrations of Tollens' reagent and citrate concentration. The blue solid lines indicate regions of bridged particles, while the red dashed lines indicate regions of raspberry particles. In between, the particles appear densely coated. Silica nanoparticles used for [Tollens'] = 25 mM and [Citrate] = 50 mM reaction conditions were slightly larger due to batch-to-batch variation of the silica core size. Scale bar is 500 nm. (For interpretation of the references to colour in this figure legend, the reader is referred to the web version of this article.)

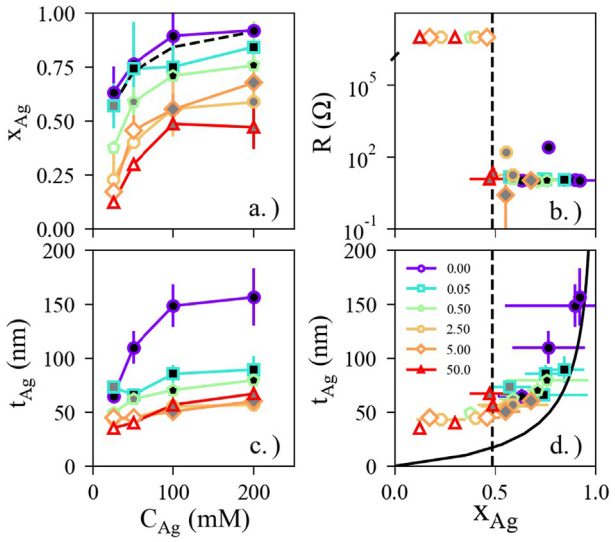

Fig. 4. (a) Silver mole fraction $x_{Ag} = x_{Ag}^{EDS} / \left(x_{Ag}^{EDS} + x_{Si}^{EDS}\right)$ as a function of Tollens' reagent concentration with the solid line approximating the estimated stoichiometric values. (b) Electrical resistance of particle thin films prepared by drop-casting on interdigitated gold electrodes with 200 μm separation. The cut-off between conductive and insulating particles occurs at approximately 0.48 silver mole fraction as indicated by the vertical dashed line. Points above the break in the y-axis are non-conductive. (c) Silver coating thickness t_{Ag} plotted as a function of Tollens' reagent concentration C_{Ag} in the reacting solution and (d) t_{Ag} vs. x_{Ag}. The solid line in (d) indicates the theoretical thickness for a completely smooth and conformal silver layer. Black filled markers represent bridged particles, grey filled symbols represent conformally coated particles, and white filled markers represent raspberry particles. The citrate concentration in mM is given in the legend.

coatings was observed is highlighted by the solid blue lines (upper left) and the region of low-density raspberry particles is highlighted by the dashed red lines (lower right) in Fig. 3. In between we observed densely packed silver deposits that conformally coat the silica nanoparticles.

EDS measurements shown in Fig. 4a further define the morphological transition and quantify changes in the amount of silver growth due to the addition of citrate. For Fig. 4a, the mole fraction of silver x_{Ag} was calculated from EDS measurements using relative silver and silica mole fractions. At least three representative regions of the SEM images were averaged for each point. The mole fraction is plotted against the Tollens' reagent concentration for each citrate concentration tested. Solid markers are used to represent conformal and bridged particles, while open symbols represent raspberry particles. The EDS results confirmed the trend observed from SEM. In addition to modifying the particle morphology and improving stability, increasing citrate concentration resulted in less silver deposited on the silica surface. In contrast, increasing the Tollens' reagent concentration increased the amount of silver deposited. Citrate's inhibition of silver deposition depended on the Tollens' reagent concentration based on quantitative comparisons of experimental to stoichiometric calculations (dashed black line in Fig. 4a). The extent of inhibition increased with increasing citrate concentration.

We performed thin-film electrical resistance measurements to quantify the transition from raspberry to conformal silver coatings as shown in Fig. 4b. Particles with uniform coverage exhibited high conductivity, while raspberry particles were non-conductive. The interconnectivity of the silver domains on the silica surface should determine the ease with which electrons can transport between those domains. Consistent with this expectation, raspberries

generally showed poor conduction. A sharp transition in conductivity is indicated by the vertical dashed line in Fig. 4b. This transition occurs at a silver mole fraction of approximately 0.48, which also conveniently delineates the morphological transition from raspberry to conformally coated particles as indicated by the closed and open symbols. To understand the origin of this transition, we performed image analysis on representative SEM images to obtain the apparent silver film thickness. The thickness of raspberry particles was estimated based on the average of the apparent particle diameter. Our analysis accounted for differences in silica nanoparticle core size between samples due to batch-to-batch variance. The results of this analysis are shown in Fig. 4c. In general, the trend was very similar to that observed for the EDS results. We observed that increasing the citrate concentration decreased the coating thickness. We also saw that in the presence of citrate, increasing the Tollens' reagent concentration had only a weak effect on the coating thickness except in the absence of citrate. These results can be conveniently summarized by depicting the relationship between the coating thickness and the silver molar ratio as shown in Fig. 4d for all samples tested. For comparison, the theoretical prediction for coating thickness calculated based on the silver mole fraction determined by EDS is shown as a solid line to Fig. 4d. This prediction agrees well with the qualitative trend evident in the figure. However, it underpredicts the apparent coating thickness at low surface coverages. An alternative model can be formulated based on the assumption that the amount of silver measured using EDS was a result of an increased number density of uniformly sized particles. This model more closely aligned with the raspberry morphology. The vertical dashed line in Fig. 4d shown at a silver mole fraction of 0.48 corresponded to a randomly close-packed monolayer of 25 nm silver spheres. This was approximately the size of silver deposits measured using SEM and was within error of the apparent coated silver thickness. These quantitative predictions closely aligned with the qualitative observations of Fig. 3 and conveniently demarcated the morphological transition from conformal to raspberry particles.

Absorbance spectroscopy is frequently used to characterize the properties of metallic nanomaterials due to the presence of the surface plasmon resonance. The plasmonic structure of the absorbance band is directly related to the metal geometry and is complementary to the microstructural characterization in Fig. 4. We therefore performed UV–Vis measurements on suspensions of nanoparticles synthesized at 25 mM Tollens' reagent concentration as a function of the citrate concentration. The results are shown in Fig. 5. At high citrate concentration, we observed plasmonic features consistent with that expected from discrete nanoparticles with an absorbance peak centred at 409.5 nm. The synthesis without citrate showed absorbance features consistent with continuous metallic films. As the citrate concentration increased, the spectra progressively blue-shifted. The peak positions are given in Table S.1. This sequence of spectra aligned qualitatively with the quantitative observations discussed in Fig. 4. It also demonstrates that citrate induces a systematic shift in morphology consistent with the observations made with SEM and EDS characterization in Fig. 4. This trend is like that observed in Chen et al as a function of reaction time [23].

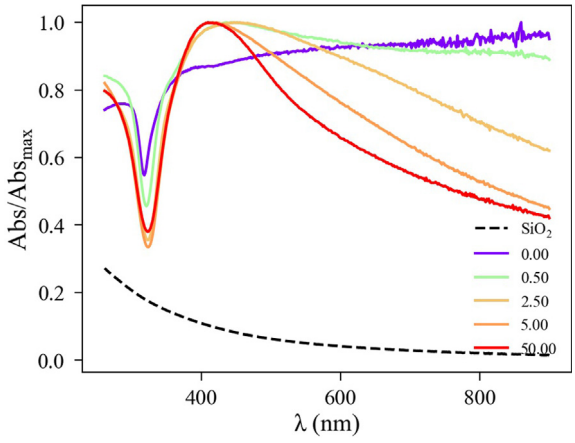

Fig. 5. UV–visible absorbance spectroscopy measurements performed on a 25 mM Tollens' reagent reaction in the presence of varying amounts of sodium citrate with concentrations indicated in the legend. The black dashed line is the absorbance from silica nanoparticles for reference.

4. Discussion

The results discussed above indicate the important role citrate plays in controlling the morphology of silver coated silica nanoparticles. However, the specific mechanism by which citrate acts to facilitate these changes remains an open question. Citrate's ability to cap silver crystals to specific sizes is well known, but this hypothesis alone cannot explain why stoichiometric deposition of silver is not achieved. We expected that the reduction of the Tollens' reagent would proceed to completion with an excess of glucose present. However, we observed a systematic decrease in the amount of silver deposited on the silica particles upon addition of citrate. One explanation is that citrate slows the rate of reaction. If the reaction were slowed significantly, then the 30-minute time interval we allowed for the reaction to occur could be insufficient for the complete reduction of Tollens' reagent.

To explore this possibility, we performed a series of otherwise identical syntheses that we terminated at different times. The results are shown in Fig. 6a and b. These reactions were terminated by submerging the reaction vial in a mixture of dry ice and ethanol and diluting the sample with cold water before imaging. It is important to note that completely halting the reaction is difficult as the reaction is rapid and thermodynamically favoured at room temperature. Nonetheless, the progression of reaction states indicated a sequence of events consistent with our experimental expectations. The first reaction was performed in the absence of citrate and is shown in Fig. 6a. Within 10 s of introducing glucose, the initial silver seeds rapidly grew into large silver deposits on the silica surface. The bridging of these silver deposits is apparent after 3 min of reaction and the film appearance remains relatively unchanged from 3 min to our standard synthesis time of 30 min. This indicates that without citrate, the reaction goes to completion very rapidly and uniform films are readily formed. This is supported by the near stoichiometric conversion at the 0 mM citrate condition shown in Fig. 4a where all reactions were performed for a 30-minute duration.

When citrate is added, it was experimentally observed that the reaction proceeds much more slowly as indicated by a slower colour change in the vial. To understand the evolution in the silver deposits during this slower rate of reaction, we performed a similar time-series experiment as in Fig. 6a but with a synthesis that contained 50 mM citrate. The results are shown in Fig. 6b. We allowed this reaction to proceed for a longer duration to test whether slower kinetics alone can explain citrate's role in modifying the silver coating morphology. In contrast to the synthesis performed without citrate, the silver deposits remained as discrete particles with only a modest increase in surface coverage after 90 min of reaction. Even after 24 h of reaction, the films remained as discrete raspberry particles without any sign of transition to conformal coating. Therefore, while slower rates of reaction can account for the lack of stoichiometric conversion of the Tollens' reagent, the morphology of the resulting particles shows a different sequence

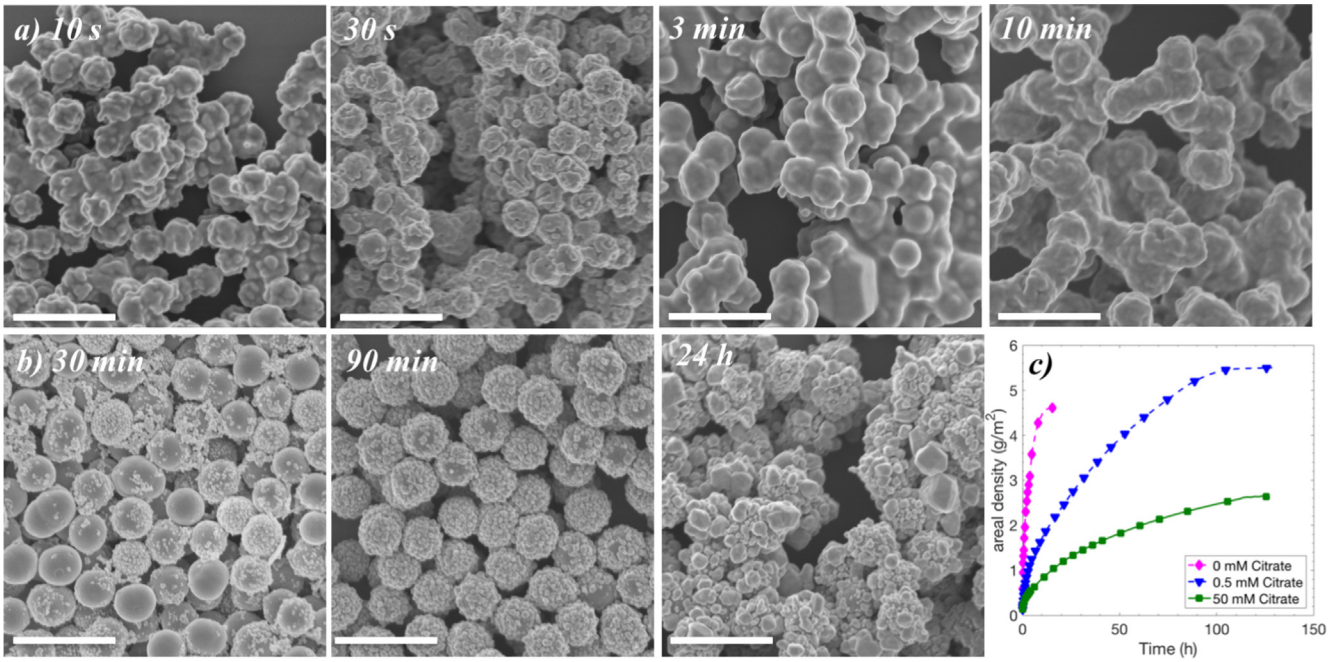

Fig. 6. (a) Different stages of silver growth for silver coated silica nanoparticles using 50 mM Tollens' reagent without any citrate at 10 s, 30 s, 3 min, and 10 min. (b) Silver growth using 25 mM Tollens' reagent and 50 mM sodium citrate for 30 min, 90 min, and 24 h. (c) In-situ QCM mass studies of silver grown on quartz crystals with 25 mM Tollens' reagent and varying sodium citrate concentrations. Scale bar is 1 μm.

of states than that observed when citrate is absent. We can then conclude that in addition to slowing the rate of reaction, citrate suppressed the merger of discrete nanoparticles into conformal films. We hypothesize that this is due to citrate's role as a capping agent. We test this hypothesis using X-Ray Diffraction (XRD) on two syntheses, one carried out at 25 mM Tollens' reagent with no citrate and the second carried out at 25 mM Tollens' regent with 50 mM citrate both with a duration of 30 min. The XRD spectra are shown in the supplemental information in Fig. S4. The spectra exhibit diffraction peaks that are identical to one another except that the reaction carried out in the presence of citrate has smaller crystallites than that carried out without citrate. The increased peak width indicates a smaller crystal grain size that supports citrate's role as a capping agent for the silver deposits on the silica surface.

To confirm the qualitative change in reaction rate observed for the reactions in Fig. 6b, a thin-film QCM study was performed. The results are shown in Fig. 6c. The reaction conditions for the QCM study consisted of 25 mM Tollens' reagent with varying citrate concentrations of 0 mM, 0.5 mM, and 50 mM. These reactions were carried out after sensitization and activation of the QCM substrates with the Tollens' reagent. As seen in Fig. 6c., increasing the citrate concentration decreased the rate of silver deposition. We allowed these experiments to continue for much longer durations and we observe deposition continuing for several days. Films grown at the 0.5 mM citrate condition resulted in the largest amount of deposited silver, followed by conditions using 0 mM citrate then 50 mM citrate. The decreased amount of deposited silver for the 0 mM citrate condition can be explained by the formation of silver nanoparticles in the bulk solution. This was not observed at any other reaction condition in our thin-film studies. These observations from QCM further confirm that citrate modified the kinetics of the reduction of the Tollens' reagent to silver metal. This behaviour has been observed previously in the synthesis of silver nanoparticles. Citrate is known to form relatively stable complexes with positively charged Ag^{+} and Ag^{2+} ions and slows their conversion to cationic silver clusters Ag_4^{2+} that are precursors to silver metal [28]. This can explain the need to increase the citrate concentration at higher Tollens' reagent concentration – the more silver present, the more citrate is needed to maintain a consistent reaction rate and thus deposited silver structure. These results emphasize the important role that citrate plays in determining the rate of reaction.

A key distinction between syntheses performed in the absence of citrate and those in the presence of large amounts of citrate is that the discrete particles do not appear to merge. If a reduced reaction rate were the only contributing factor to the observed morphological diversity in silver deposits, then we would still anticipate that the discrete silver deposits would eventually grow large enough and merge to form conformal films. Our results at the 50 mM citrate condition suggest that this is not the case. These observations combined with the XRD results confirm that citrate plays a dual role in both reducing the rate of reduction of the Tollens' reagent and in inhibiting the fusion of distinct silver particles on the silica surface. We believe it is the combination of these two factors, (1) slower rate of reduction of the Tollens' reagent and (2) hindered fusion of discrete nanoparticles on the silica surface that provide the morphological control that we demonstrate in this work.

5. Conclusions

We have employed a modified silver mirroring reaction to deposit silver onto the surface of silica nanoparticles. We demonstrated that the modified synthesis procedure resulted in conformally coated particles and that tin sensitization was a key step to achieving this morphology. We also observed significant bridging of these conformally coated silica particles, which was mitigated upon the addition of citrate. Citrate had a dramatic effect on both the silver morphology and kinetics of reaction, which we thoroughly characterized with spectroscopy, electron microscopy, and QCM. We used these results to understand the role of citrate in mediating the silver coating morphology and we found that

citrate caps and restricts silver growth while reducing the reaction rate. Importantly, through proper selection of reaction conditions we found that it was possible to form silver coated silica nanoparticles that were electrically conductive and unbridged, which are excellent candidates for applications in composites and electrical devices. While this work focused mainly on the morphological control of silver deposits on spherical nanoparticles, the approaches used here should be generalizable to any negatively charged surface. Additionally, the use of citrate for this approach is particularly relevant to applications that exploit the electrical and catalytic properties of silver when it is deposited on nano-scale structures as citrate can be subsequently removed.

CRediT authorship contribution statement

Jeffrey E. Chen: Conceptualization, Methodology, Writing - original draft, Writing - review & editing. **Qifeng Wang:** Data curation, Writing - original draft. **Kenneth R. Shull:** Project administration. **Jeffrey J. Richards:** Supervision, Writing - review & editing.

Declaration of Competing Interest

There are no conflicts to declare.

Acknowledgements

Funding for this work was provided in part by Northwestern University and J. Chen would like to thank the Murphy Fellow's program for partial support during this period. This work made use of the EPIC facility of Northwestern University's NUANCE Center, which has received support from the Soft and Hybrid Nanotechnology Experimental (SHyNE) Resource (NSF ECCS-1542205); the MRSEC program (NSF DMR-1720139) at the Materials Research Center; the International Institute for Nanotechnology (IIN); the Keck Foundation; and the State of Illinois, through the IIN. This work made use of the Jerome B. Cohen X-Ray Diffraction Facility supported by the MRSEC program of the National Science Foundation (DMR-1720139) at the Materials Research Center of Northwestern University.

Appendix A. Supplementary material

Supplementary data to this article can be found online at https://doi.org/10.1016/j.jcis.2020.05.024.

References

[1] J.J. Chen, J. Zhang, Y. Wang, Y.L. Guo, Z.S. Feng, A particle-free silver precursor ink useful for inkjet printing to fabricate highly conductive patterns, J. Mater. Chem. C. 4 (2016) 10494–10499, https://doi.org/10.1039/c6tc03719d.
[2] B.Y. Ahn, E.B. Duoss, M.J. Motala, X. Guo, S. Il Park, Y. Xiong, J. Yoon, R.G. Nuzzo, J.A. Rogers, J.A. Lewis, Omnidirectional printing of flexible, stretchable, and spanning silver microelectrodes, Science (80-.) 323 (2009) 1590–1593, https://doi.org/10.1126/science.1168375.
[3] S.J. Oldenburg, S.L. Westcott, R.D. Averitt, N.J. Halas, Surface enhanced Raman scattering in the near infrared using metal nanoshell substrates, J. Chem. Phys. 111 (1999) 4729–4735, https://doi.org/10.1063/1.479235.
[4] Y. Mao, M. Zhu, W. Wang, D. Yu, Well-defined silver conductive pattern fabricated on polyester fabric by screen printing a dopamine surface modifier followed by electroless plating, Soft Matter 14 (2018) 1260–1269, https://doi.org/10.1039/c7sm02246h.
[5] J. Cai, M. Zhang, Z. Sun, C. Zhang, C. Liang, A. Khan, X. Ning, H. Ge, S.P. Feng, W. Di Li, Highly-facile template-based selective electroless metallization of micro- and nanopatterns for plastic electronics and plasmonics, J. Mater. Chem. C. 7 (2019) 4363–4373, https://doi.org/10.1039/c8tc06354k.
[6] A. Radke, T. Gissibl, T. Klotzbücher, P.V. Braun, H. Giessen, Three-dimensional bichiral plasmonic crystals fabricated by direct laser writing and electroless silver plating, Adv. Mater. 23 (2011) 3018–3021, https://doi.org/10.1002/adma.201100543.
[7] Y. Shacham-Diamand, T. Osaka, Y. Okinaka, A. Sugiyama, V. Dubin, 30 Years of electroless plating for semiconductor and polymer micro-systems, Microelectron. Eng. 132 (2015) 35–45, https://doi.org/10.1016/j.mee.2014.09.003.
[8] H.D. Curtis, Methods of Silvering Mirrors, Publ. Astron. Soc. Pac. 23 (1911) 13–32.
[9] A. Lahiri, G. Pulletikurthi, F. Endres, A review on the electroless deposition of functional materials in ionic liquids for batteries and catalysis, Front. Chem. 7 (2019) 1–13, https://doi.org/10.3389/fchem.2019.00085.
[10] X. Wei, D.K. Roper, Tin sensitization for electroless plating review, J. Electrochem. Soc. 161 (2014) D235–D242, https://doi.org/10.1149/2.047405jes.
[11] A. Dokoutchaev, J. Thomas James, S.C. Koene, S. Pathak, G.K. Surya Prakash, M. E. Thompson, Colloidal metal deposition onto functionalized polystyrene microspheres, Chem. Mater. 11 (1999) 2389–2399, https://doi.org/10.1021/cm9900352.
[12] D. Zhang, L. Qi, J. Ma, H. Cheng, Synthesis of submicrometer-sized hollow silver spheres in mixed polymer-surfactant solutions, Adv. Mater. 14 (2002) 1499–1502, https://doi.org/10.1002/1521-4095(20021016)14:20<1499::AID-ADMA1499>3.0.CO;2-5.
[13] Z. Deng, M. Chen, L. Wu, Novel method to fabricate SiO2/Ag composite spheres and their catalytic, surface-enhanced raman scattering properties, J. Phys. Chem. C. 111 (2007) 11692–11698, https://doi.org/10.1021/jp073632h.
[14] H. Chang, E. Ko, H. Kang, M.G. Cha, Y.S. Lee, D.H. Jeong, Synthesis of optically tunable bumpy silver nanoshells by changing the silica core size and their SERS activities, RSC Adv. 7 (2017) 40255–40261, https://doi.org/10.1039/c7ra06170f.
[15] D.H. Jiang, P.C. Tsai, C.C. Kuo, F.C. Jhuang, H.C. Guo, S.P. Chen, Y.C. Liao, T. Satoh, S.H. Tung, Facile preparation of Cu/Ag core/shell electrospun nanofibers as highly stable and flexible transparent conductive electrodes for optoelectronic devices, ACS Appl. Mater. Interfaces. 11 (2019) 10118–10127, https://doi.org/10.1021/acsami.8b18366.
[16] X. Cauchy, D. Therriault, Synthesis of highly conductive, uniformly silver-coated carbon nanofibers by electroless deposition, ACS Appl. Mater. Interfaces. 9 (2017) 29010–29020, https://doi.org/10.1021/acsami.7b06526.
[17] P.K. Jain, X. Huang, I.H. El-Sayed, M.A. El-Sayed, Noble metals on the nanoscale: Optical and photothermal properties and some applications in imaging, sensing, biology, and medicine, Acc. Chem. Res. 41 (2008) 1578–1586, https://doi.org/10.1021/ar7002804.
[18] M. Rycenga, C.M. Cobley, J. Zeng, W. Li, C.H. Moran, Q. Zhang, D. Qin, Y. Xia, Controlling the synthesis and assembly of silver nanostructures for plasmonic applications, Chem. Rev. 111 (2011) 3669–3712, https://doi.org/10.1021/cr100275d.
[19] N. Fang, H. Lee, C. Sun, X. Zhang, Sub-diffraction-limited optical imaging with a silver superlens, Science (80-.) 308 (2005) 534–537, https://doi.org/10.1126/science.1108759.
[20] V.A. Online, S. Agnihotri, S. Mukherji, S. Mukherji, Size-controlled silver nanoparticles synthesized over the range 5–100 nm using the same protocol and their antibacterial effica, RSC Adv. (2014).
[21] N.G. Bastús, F. Merkoçi, J. Piella, V. Puntes, Synthesis of highly monodisperse citrate-stabilized silver nanoparticles of up to 200 nm: Kinetic control and catalytic properties, Chem. Mater. 26 (2014) 2836–2846, https://doi.org/10.1021/cm500316k.
[22] M. Testa-Anta, M.A. Correa-Duarte, V. Salgueiriño, Self-assembly of spherical or rod-shaped magnetic nanocrystals onto curved substrates governed by the radius of curvature, Part. Part. Syst. Charact. 35 (2018) 1–5, https://doi.org/10.1002/ppsc.201800046.
[23] H.Y. Chen, H.P. Shen, H.C. Wu, M.S. Wang, C.F. Lee, W.Y. Chiu, W.C. Chen, Synthesis of monodispersed polystyrene-silver core-shell particles and their application in the fabrication of stretchable large-scale anisotropic conductive films, J. Mater. Chem. C. 3 (2015) 3318–3328, https://doi.org/10.1039/c4tc02918f.
[24] J. Zhang, J. Liu, S. Wang, P. Zhan, Z. Wang, N. Ming, Facile methods to coat polystyrene and silica colloids with metal, Adv. Funct. Mater. 14 (2004) 1089–1096, https://doi.org/10.1002/adfm.200400119.
[25] Z. Chen, Z.L. Wang, P. Zhan, J.H. Zhang, W.Y. Zhang, H.T. Wang, N.B. Ming, Preparation of metallodielectric composite particles with multishell structure, Langmuir 20 (2004) 3042–3046, https://doi.org/10.1021/la035326a.
[26] W. Wang, R. Li, M. Tian, L. Liu, H. Zou, X. Zhao, L. Zhang, Surface silverized meta-aramid fibers prepared by bio-inspired poly(dopamine) functionalization, ACS Appl. Mater. Interfaces. 5 (2013) 2062–2069, https://doi.org/10.1021/am302956h.
[27] K.M. Koczkur, S. Mourdikoudis, L. Polavarapu, S.E. Skrabalak, Polyvinylpyrrolidone (PVP) in nanoparticle synthesis, Dalt. Trans. 44 (2015) 17883–17905, https://doi.org/10.1039/c5dt02964c.
[28] K. Ranoszek-Soliwoda, E. Tomaszewska, E. Socha, P. Krzyczmonik, A. Ignaczak, P. Orlowski, M. Krzyzowska, G. Celichowski, J. Grobelny, The role of tannic acid and citrate in the synthesis of silver nanoparticles, J. Nanoparticle Res. 19 (2017), https://doi.org/10.1007/s11051-017-3973-9.
[29] Q. Zhang, N. Li, J. Goebl, Z. Lu, Y. Yin, A systematic study of the synthesis of silver nanoplates: Is citrate a "magic" reagent?, J. Am. Chem. Soc. 133 (2011) 18931–18939, https://doi.org/10.1021/ja2080345.
[30] K.M. Chen, Mechanism of hypophosphite-reduced electroless copper plating, J. Electrochem. Soc. 136 (1989) 72–75, https://doi.org/10.1149/1.2096617.
[31] J. Li, P.A. Kohl, The deposition characteristics of accelerated nonformaldehyde electroless copper plating, J. Electrochem. Soc. 150 (2003) 558–562, https://doi.org/10.1149/1.1591760.

[32] G.L. Agawane, S.W. Shin, A.V. Moholkar, K.V. Gurav, J.H. Yun, J.Y. Lee, J.H. Kim, Non-toxic complexing agent Tri-citrate's effect on chemical bath deposited ZnS thin films and its growth mechanism, J. Alloys Compd. 535 (2012) 53–61, https://doi.org/10.1016/j.jallcom.2012.04.073.
[33] E. Chassaing, M. Cherkaoui, A. Srhiri, Electrochemical investigation of the autocatalytic deposition of Ni-Cu-P alloys, J. Appl. Electrochem. 23 (1993) 1169–1174, https://doi.org/10.1007/BF00625591.
[34] T.J. Whang, M.T. Hsieh, Y.C. Kao, Studies of single-step electrodeposition of CuInSe 2 thin films with citrate as a complexing agent, Appl. Surf. Sci. 257 (2010) 1457–1462, https://doi.org/10.1016/j.apsusc.2010.08.072.
[35] F. Chraibi, M. Fahoume, A. Ennaoui, J.L. Delplancke, Influence of citrate ions as complexing agent for electrodeposition of CuInSe2 thin films, Phys. Status Solidi Appl. Res. 186 (2001) 373–381, https://doi.org/10.1002/1521-396X(200108)186:3<373::AID-PSSA373>3.0.CO;2-D.
[36] J.H. Cha, W.J. Woo, S.C. Jeong, S. Jung, H.J. Lee, D.Y. Jung, Complexing agent-assisted highly dense CuInSe2 thin films prepared by one-step electrochemical deposition, J. Electroanal. Chem. 808 (2018) 211–217, https://doi.org/10.1016/j.jelechem.2017.12.004.
[37] J. Singh, R. Poolla, Effect of complexing agents on properties of electrodeposited InSb thin films, J. Electron. Mater. 47 (2018) 6848–6861, https://doi.org/10.1007/s11664-018-6608-8.
[38] Y. Kobayashi, V. Salgueiriño-Maceira, L.M. Liz-Marzán, Deposition of silver nanoparticles on silica spheres by pretreatment steps in electroless plating, Chem. Mater. 13 (2001) 1630–1633, https://doi.org/10.1021/cm001240g.
[39] E. Bohn, Werner Stober, Arthur Fink, Controlled growth of monodisperse silica spheres in the micron size range, J. Colloid Interface Sci. 69 (1968) 62–69.
[40] S. Durmazel, A. Üzer, B. Erbil, B. Sayln, R. Apak, Silver nanoparticle formation-based colorimetric determination of reducing sugars in food extracts via Tollens' reagent, ACS Omega 4 (2019) 7596–7604, https://doi.org/10.1021/acsomega.9b00761.
[41] I.D. Jenkins, Tollens' test, fulminating silver, and silver fulminate, J. Chem. Educ. 64 (1987) 164, https://doi.org/10.1021/ed064p164.
[42] H. Ohshima, T.W. Healy, L.R. White, Accurate analytic expressions for the surface charge density/surface potential relationship and double-layer potential distribution for a spherical colloidal particle, J. Colloid Interface Sci. 90 (1982) 17–26, https://doi.org/10.1016/0021-9797(82)90393-9.
[43] H. Ohshima, Approximate analytic expression for the electrophoretic mobility of a spherical colloidal particle, J. Colloid Interface Sci. 239 (2001) 587–590, https://doi.org/10.1006/jcis.2001.7608.
[44] Q. Wang, M. Yang, K.R.S. Shull, Python program for QCM data acquisition and analysis, Zenodo. (2018), https://doi.org/10.5281/zenodo.2486039.
[45] G. Sauerbrey, Verwendung von Schwingquarzen zur Wägung dünner Schichten und zur Mikrowägung, Zeitschrift Für Phys. 155 (1959) 206–222, https://doi.org/10.1007/BF01337937.
[46] R.L. Cohen, B.T. Laboratories, M. Hi, M6ssbauer Study of Tin (Il) Sensitizer Deposits on Kapton, J. Electrochem Soc. (1971) 2042–2046.
[47] R.L. Cohen, K.W. West, B.T. Laboratories, M. Hill, Solution chemistry and colloid formation in the tin chloride sensitizing process, J. Electrochem Soc. 119 (1972) 2–7.
[48] C.H. de Minjer, P.F.J.v.d. Boom, Nucleation with SnCl2-PdCl2 solutions of glass before electroless plating, J. Electrochem. Soc. 120 (1973) 1644–1650, https://doi.org/10.1149/1.2403321.
[49] J. Boehm, A. François, H. Ebendorff-Heidepriem, T.M. Monro, Chemical deposition of silver for the fabrication of surface plasmon microstructured optical fibre sensors, Plasmonics. 6 (2011) 133–136, https://doi.org/10.1007/s11468-010-9178-z.
[50] W. Wang, Y. Jiang, Y. Liao, M. Tian, H. Zou, L. Zhang, Fabrication of silver-coated silica microspheres through mussel-inspired surface functionalization, J. Colloid Interface Sci. 358 (2011) 567–574, https://doi.org/10.1016/j.jcis.2011.03.023.
[51] Y. Xia, N. Venkateswaran, D. Qin, J. Tien, G.M. Whitesides, Use of electroless silver as the substrate in microcontact printing of alkanethiols and its application in microfabrication, 1998. https://pubs.acs.org/sharingguidelines (accessed August 20, 2019).